OBSERVATION, THEORETICAL CALCULATION AND ANALYSIS OF THE SOLAR FLARE ON MAY 11, 2012

© 2025 Yu.A. Kupryakov [1,2*], K.V. Bychkov [1], O.M. Belova [3], A.B. Gorshkov [1], V.A. Malyutin [3]**

[1] *Sternberg Astronomical Institute of Lomonosov Moscow State University (SAI MSU), Moscow, Russia*

[2] *Astronomical Institute of the Czech Academy of Sciences, Ondřejov, Czech Republic*

[3] *Faculty of Physics of Lomonosov Moscow State University (MSU), Moscow, Russia*

**e-mail: kupry@asu.cas.cz*

***e-mail: malyutinv@list.ru*

Received March 07 , 2024

Revised July 17, 2024

Accepted for publication December 12, 2024

The solar flare of May 11, 2012 was observed using two spectrographs of the Astronomical Institute of the Czech Academy of Sciences: MFS – multichannel flare spectrograph and HSFA – horizontal solar research facility. After processing the spectra, the integral radiation fluxes in the hydrogen, helium, and calcium lines were determined. Within the framework of a heated gas model, a theoretical calculation of plasma parameters was performed, taking into account the physical conditions in the chromosphere, including self-absorption in spectral lines. Comparison across six lines at once made it possible to reconstruct the temperature, density, and spatial structure of the radiating gas with a high degree of confidence. Simultaneously, a search for quasi-periodic pulsations of radiation in the studied flare was conducted, which showed the absence of such pulsations in almost all spectral ranges. The exception was the detection of pulsations in chromospheric images at the spectrograph slit in the Hα line with a period of 30 seconds.

Keywords: chromosphere, solar flare, quasi-periodic pulsations

DOI: 10.31857/S00167940250301e4

1. INTRODUCTION

At the beginning of the flare process, emission in the H α line appears in separate bright nodes, which then, as the flare develops, merge into extended luminous ribbons. Usually, the flare emission ribbons are shifted relative to each other, and the distance between them increases during its development. According to modern concepts, this indicates an upward movement of the energy release zone at the top of the magnetic arcade, where the current sheet is located.

It is believed that part of the released energy (the main energy release of the flare is localized in the lower corona) in the form of fast particles and hot plasma flows with possible formation of shock waves, propagates downward into the chromosphere. In the solar chromosphere, under the influence of fast particles, secondary manifestations of the flare arise – the glow of flare ribbons in the optical and X-ray spectral ranges with subsequent ejection of heated plasma upward from the chromosphere ("chromospheric evaporation") [Borovik et al., 2019].

Chromospheric oscillations can give us an idea of the physical environment of the solar atmosphere, both under quiet Sun conditions and during a flare. Many authors report an increase in the prevalence of three-minute oscillations, which are believed to be excited by events affecting the chromosphere, such as flares.

Velocity oscillations were detected throughout the active region both before and after the flare, but were distinctly observed in areas illuminated by the second flare. When compared with EUV images (EUV – *extreme ultraviolet*), it was seen that strong chromospheric velocity oscillations with periods of 3–4 min occurred at the same time and in the same location as the flare loop cooling 30 minutes after the second flare peak. This could be evidence of disturbances in the loop exciting a chromospheric response at its acoustic cutoff frequency [Millar et al., 2024].

The aim of this work is to determine the physical parameters of the plasma and attempt to detect quasi-periodic oscillations during the flare process.

2. OBSERVATIONS AND PROCESSING

All spectral observations of the solar flare on May 11, 2012 (internationally designated as SOL2012-05-11), which occurred in the active region NOAA 11475 of class C4.7 began at 12:58, reached its maximum at 13:10 UT and ended at 13:42 UT (an example of the flare filtergram is shown in Fig. 1), – were obtained by us at the Czech Academy of Sciences Observatory (Ondřejov) using the spectrographs *Multichannel-Flare-Spectrograph* (MFS, 230 mm/13.5 m) and *Horizontal-Sonnen-Forschungs-Anlage* (HSFA-2, 500 mm/35m). To search for quasi-periodic pulsations, we used X-ray flare observation data from *Ramaty High Energy Solar Spectroscope Imager* (RHESSI),

FERMI/GBM and microwave emission data from *Radio Solar Telescope Network* (RSTN), as well as data from the RT3 3.0 GHz radio telescope (Ondřejov Observatory) and the GOES spacecraft.

Fig. 1.

Fig. 2.

We studied the behavior of emission intensity curves in the H CaII (λ = 3968 Å), Hε, Hβ, HeI D3, Hα and Ca IR (λ = 8542 Å) lines (example shown in Fig. 2) during the flare development and compared the results with calculated values. All spectral observations in these lines were performed using the HSFA-2 spectrograph (*Horizontal-Sonnen-Forschungs-Anlage-2*). To determine possible emission mechanisms in the lines, the radiation flux was calculated. We performed calculations within the framework of a model consisting of homogeneous gas layers, adjusting their parameters so that the theoretical radiation fluxes were close to the observed ones. After data reduction, line profiles in the active and quiet regions of the chromosphere were obtained, and radiation flux values were determined (see Fig. 3 for example profiles). The flux values in all spectral lines in erg $cm^{-2} s^{-1}$ for 7 investigated time moments in the interval 13:03:13−13:13:17 UT are given in Table 1.

Fig. 3.

Table 1.

3. CALCULATION RESULTS

Calculations of the ionization state and radiation fluxes in a model of chromospheric gas have been performed, specifically, gas that is transparent in the continuous spectrum of the optical range, but possibly experiencing self-absorption at the frequencies of spectral lines. Balance equations are written for 18 levels of the hydrogen atom, 29 levels of the helium atom, and 22 levels of the CaII ion. When calculating populations, bound-free, free-bound, and bound-bound collisional and radiative transitions were taken into account: atomic data for hydrogen were taken from [Johnson, 1972], atomic data for helium were obtained as a result of the ATOM program [Vainstein and Shevelko, 1983], atomic data for calcium - from the National Institute of Standards and Technology (NIST) for energy levels and transition probabilities, from Melendez et al., 2007 for collisional excitation/deactivation, from Seaton [1964] for collisional ionization. The calculation of radiation transfer was performed within the framework of the Sobolev-Holstein-Biberman photon escape probability model [Biberman, 1947; Holstein, 1947, 1951]; for the lines of the helium atom and CaII ion, a Voigt profile was used, for the hydrogen atom - a convolution of Doppler and Holtsmark profiles. Photospheric radiation is simulated by a black body model with a temperature of 5500 °K.

The observed emission spectra of the Balmer series of hydrogen and the D3 line of helium confirm the strong heterogeneity of the gas and a significant velocity dispersion. All episodes except

the last one can be explained using a model of two stationary layers: one closer to the observer (C) and one further from the observer (F). The emission from the layers combines, with the closer layer partially absorbing the radiation from the further layer in the lines of the Balmer series of hydrogen and CaII. The theoretical parameters of the layers for all seven episodes do not differ significantly; they are presented in Table 2. Here, the first layer is the further one, and the second is the closer one to the observer. The Lyman series of hydrogen has a strong influence on the photoionization of CaII. We simulate this influence with the parameter T_{Ly}, which is essentially a black body temperature and is measured in Kelvin. The relatively flat Balmer decrement (Hα/Hβ < 1.6) is a consequence of self-absorption in the Hα line. To explain the decrement at 13:13:17 (Table 2), a set of three layers is required: close (C), middle (M), and far (F). The parameters of the third, closest layer are N3 = $9.0 \cdot 10^{12}$ cm^{-3}, *h3* = 10 km, *T* 3 = 6500 °K, *v3* = 7.5 km/s. The HeI 5876 Å line and high fluxes in the Balmer series lines are formed in the hot far layer. The middle layer absorbs Balmer lines and creates emission in the CaII ion lines. The close layer creates the main emission power of the transparent gas in the Balmer lines.

Table 2.

Table 3.

Fig. 4.

Theoretical line fluxes are given in Table 3. It can be seen that it is possible to approximate the theoretical relative values to the observed ones, but the absolute values turn out to be several (up to 10) times smaller than the observed ones. This can be explained in a cloud structure model: we see the combined radiation from a group of two- (three-)layer clouds, with the number of these clouds being inversely proportional to the contribution of an individual cloud to the total flux. The observed and theoretical fluxes are shown in Fig. 4.

4. SEARCH FOR QUASI-PERIODIC PULSATIONS

At our disposal were data from X-ray observations of flares from RHESSI and FERMI/GBM (*Fermi Gamma-ray Space Telescope*), microwave emission data from RSTN, as well as data from the RT3 3.0 GHz radio telescope (Ondřejov Observatory) and the GOES apparatus.

Signal graphs and their spectra show only white noise, independent of frequency. The characteristic linear rise of the spectrum from high frequencies to low ones ("red noise") is not observed either on the linear graph or on the logarithmic one. Therefore, it is impossible to find quasi-periodic pulsations here. The exception is the detection of pulsation from chromosphere images in the Hα line with a period of 30 s (Fig. 5, Fig. 6).

Fig. 5.

Fig. 6.

5. CONCLUSIONS

1. The theoretical values of relative radiation fluxes in spectral lines can be approximated to the observed ones only when the theoretical absolute fluxes are several times less than the observed absolute fluxes.

2. Based on the first point, the following model of luminous gas is proposed: the radiation of the object is composed of many relatively small clouds with a size of about 100 km along the line of sight.

3. The simultaneous presence in the spectrum of noticeable emission in the D3 line of the helium atom and the resonance line H of the CaII ion requires for its explanation a model of inhomogeneous clouds, each of which contains at least two layers with different temperature and gas concentration.

4. The good agreement of relative fluxes in the lines between Table 1 and Table 3 shows that we possibly observe the emission of approximately ten dispersing clouds. There are exactly 10 clouds because the measured absolute fluxes from Table 1 exceed the theoretical ones from Table 3 by about an order of magnitude.

5. The gas concentrations of the clouds exceed those in prominences by orders of magnitude. Such clouds could not have formed from prominences. The most likely area of cloud formation is the chromosphere at a height of no more than 500-1000 km.

6. The search for quasi-periodic pulsations in the SOL2012-05-11 flare showed their absence in almost all spectral ranges. The exception is the detection of pulsation from chromosphere images in the Hα line with a period of 30 seconds.

ACKNOWLEDGMENTS

The authors thank the teams of RHESSI, GOES, SDO, and Ondřejov Observatory for the opportunity to conduct observations and use the data.

FUNDING

The work was carried out at the authors' expense.

REFERENCES

– *Biberman L.M.* On the theory of diffusion of resonance radiation // JETP. V. 17. P. 416–430. 1947.

– *Borovik A., Golovko A., Polyakov V., Trifonov V., Yazev S* . Solar activity research at the Baikal Astrophysical Observatory of ISTP SB RAS. // SOLNECHNO-ZEMNAYA FIZIKA. V. 5. N 3. 2019. https://doi.org./10.12737/szf-53201903

– *Holstein T.* Imprisonment of resonance radiation in gases // Phys. Rev. V. 72. P. 1212–1233. 1947.

– *Holstein T.* Imprisonment of resonance radiation in gases. II // Phys. Rev. V. 83 P. 1159–1168. 1951.

– *Johnson L. C.* Approximations for collisional and radiative transition rates in atomic hydrogen. //Astrophys. J. V. 174. P. 227–236. 1972.

– *Melendez M., Bautista M.A., Badnell N.R.* Atomic data from the IRON project. LXIV. Radiative transition rates and collisional strengths of CaII. // Astron. Astrophys. V. 469. Iss. 3. P. 1203–1209. 2007.

– *Millar D. C. L., Fletcher L., Joshi J.* Intensity and velocity oscillations in a flaring active region. //

– Monthly Notices of the Royal Astronomical Society. V. 527. Iss. 3. P. 5916–5928. 2024.

– *Seaton M.J.* The spectrum of the solar corona // Planet. Space Sci. V. 12. P. 55–74. 1964.

– *Vainstein L. A., Shevelko V. P.* Program ATOM for calculation of atomic characteristics. // Preprint of the Lebedev Physical Institute N. 19. Moscow, 1983.

Table 1. Observed absolute fluxes (in units of erg cm $^{-2}$ s $^{-1}$) in 6 investigated spectral lines: Hα, Hβ, Hε, H, IR CaII and D3 and relative fluxes Hα/Hβ, Hε/Hβ, Hα/H CaII, H/IR CaII, Hα/D3 (in units of erg cm $^{-2}$ s $^{-1}$).

Spectral lines	UT episode						
	13:03:33	13:04:06	13:04:56	13:05:31	13:08:32	13:09:06	13:13:17
Hα	$3.17\cdot10^{7}$	$3.00\cdot10^{7}$	$1.82\cdot10^{7}$	$2.27\cdot10^{7}$	$2.47\cdot10^{7}$	$1.59\cdot10^{7}$	$1.50\cdot10^{7}$
Hβ	$2.70\cdot10^{7}$	$2.44\cdot10^{7}$	$1.52\cdot10^{7}$	$1.67\cdot10^{7}$	$2.02\cdot10^{7}$	$1.10\cdot10^{7}$	$9.44\cdot10^{6}$
Hα/Hβ	1.17	1.23	1.20	1.36	1.22	1.35	1.59
Hε	$9.76\cdot10^{6}$	$9.57\cdot10^{6}$	$4.81\cdot10^{6}$	$5.71\cdot10^{6}$	$5.56\cdot10^{6}$	$3.24\cdot10^{6}$	$2.76\cdot10^{6}$
Hε/Hβ	0.36	0.39	0.32	0.34	0.28	0.27	0.29
H CaII	$2.76\cdot10^{7}$	$2.68\cdot10^{7}$	$1.64\cdot10^{7}$	$1.77\cdot10^{7}$	$1.35\cdot10^{7}$	$1.37\cdot10^{7}$	$1.08\cdot10^{7}$
Hα/H CaII	1.15	1.12	1.11	1.28	2.09	1.16	1.39
IR CaII	$1.40\cdot10^{7}$	$1.38\cdot10^{7}$	$1.02\cdot10^{7}$	$1.21\cdot10^{7}$	$1.18\cdot10^{7}$	$9.70\cdot10^{6}$	$8.24\cdot10^{6}$
H/IR CaII	1.97	1.94	1.61	1.46	1.14	1.41	1.31
D3	$1.73\cdot10^{6}$	$1.47\cdot10^{6}$	$9.36\cdot10^{5}$	$1.11\cdot10^{6}$	$2.87\cdot10^{5}$	$1.42\cdot10^{6}$	$1.55\cdot10^{6}$
Hα/D3	18.3	20.4	19.4	20.4	86.1	11.2	9.68

Table 2. Parameters of emitting layers.

Layer Parameters	UT of Episode						
	13:03:33	13:04:06	13:04:56	13:05:31	13:08:32	13:09:06	13:13:17
N1, cm^{-3}	$1.0 \cdot 10^{12}$	$1.0 \cdot 10^{12}$	$1.0 \cdot 10^{12}$	$5.0 \cdot 10^{11}$	$5.0 \cdot 10^{11}$	$6.0 \cdot 10^{11}$	$8.0 \cdot 10^{12}$
N2, cm^{-3}	$3.0 \cdot 10^{12}$	$3.0 \cdot 10^{12}$	$6.0 \cdot 10^{12}$	$8.0 \cdot 10^{12}$	$4.0 \cdot 10^{12}$	$4.0 \cdot 10^{12}$	$1.0 \cdot 10^{12}$
h1 , km	60	60	60	100	100	100	100
h2 , km	40	40	40	120	100	100	100
T1, °K	18000	18000	18000	18000	14000	18000	7450
T2, °K	9000	8500	8200	7100	7750	7750	18000
v1 , km/s	3.0	3.0	3.0	3.0	3.0	3.0	5.8
v2 , km/s	6.0	4.5	5.0	3.0	1.8	3.5	3.0
T_{Ly}, °K	6200	7000	7200	8100	7500	7500	7700
N3, cm^{-3}	–	–	–	–	–	–	$9.0 \cdot 10^{12}$
h3 , km	–	–	–	–	–	–	10
T3, °K	–	–	–	–	–	–	6500
v3 , km/s	–	–	–	–	–	–	7.5

Note. N1, N2, N3 – concentration of layers 1, 2 and 3; *h1, h2, h3* – height of layers; T1, T2, T3 – temperature; *v1, v2, v3* - radial velocity; T °Ly – temperature of the Lyman series of hydrogen.

Table 3. Theoretical absolute fluxes in 6 studied spectral lines and relative fluxes, as in Table 1 (in units of erg cm $^{-2}$ s $^{-1}$).

Spectral lines	UT episode						
	13:03:33	13:04:06	13:04:56	13:05:31	13:08:32	13:09:06	13:13:17
Hα	$3.08\cdot10^{6}$	$2.06\cdot10^{6}$	$2.76\cdot10^{6}$	$1.20\cdot10^{6}$	$1.59\cdot10^{6}$	$1.62\cdot10^{6}$	$2.99\cdot10^{6}$
Hβ	$2.73\cdot10^{6}$	$1.65\cdot10^{6}$	$2.35\cdot10^{6}$	$9.04\cdot10^{5}$	$1.25\cdot10^{6}$	$1.27\cdot10^{6}$	$1.94\cdot10^{6}$
Hα/Hβ	1.13	1.25	1.17	1.33	1.27	1.28	1.54
Hε	$7.36\cdot10^{5}$	$3.79\cdot10^{5}$	$7.55\cdot10^{5}$	$2.18\cdot10^{5}$	$3.62\cdot10^{5}$	$3.59\cdot10^{5}$	$5.68\cdot10^{5}$
Hε/Hβ	0.27	0.23	0.32	0.24	0.29	0.28	0.29
H CaII	$2.96\cdot10^{6}$	$1.80\cdot10^{6}$	$2.42\cdot10^{6}$	$1.02\cdot10^{6}$	$7.90\cdot10^{5}$	$1.36\cdot10^{6}$	$2.22\cdot10^{6}$
Hα/H CaII	1.04	1.15	1.14	1.18	2.01	1.20	1.35
IR CaII	$2.01\cdot10^{6}$	$9.77\cdot10^{5}$	$1.84\cdot10^{6}$	$7.59\cdot10^{5}$	$7.74\cdot10^{5}$	$1.03\cdot10^{6}$	$1.93\cdot10^{6}$
H CaII/IR CaII	1.47	1.84	1.31	1.34	1.02	1.32	1.15
D3	$2.01\cdot10^{5}$	$1.68\cdot10^{5}$	$1.68\cdot10^{5}$	$1.13\cdot10^{5}$	$1.76\cdot10^{4}$	$1.45\cdot10^{5}$	$2.63\cdot10^{5}$
Hα/D3	15.3	12.2	16.4	10.6	90.3	11.2	11.3

Figure captions

Fig. 1. Filtergram in Hα line at 13:07 UT. The vertical white line corresponds to the spectrograph slit, two horizontal lines are reference marks used to link the filtergram to the spectra.

Fig. 2. Filtergram in Hα line (1) and spectra of H CaII and Hε; Hβ; HeI D3; Hα; Ca IR 8542 Å lines (panels 2-6) at 13:13 UT.

Fig. 3. Example of changes in the H CaII and Hε line profiles in the time interval 13:03:33 - 13:14:43 UT, as well as the profile for the quiet Sun

Fig. 4. Radiation fluxes in spectral lines at selected time points

Fig. 5. Pulsation spectrum determined from chromospheric images in the Hα line. The axes of periods P in minutes and amplitude A in arbitrary units are given on a logarithmic scale. Arrows indicate: 1 – signal spectrum; 2 – linear regression drawn through the signal; 3 – noise level; 4 – 90% significance level

Fig. 6. Spectrum of the flux on the spectrograph slit in the Hα line. The solid line indicates the signal spectrum, and the dashed line indicates the 90% significance level in arbitrary units. The period axis is given in minutes.

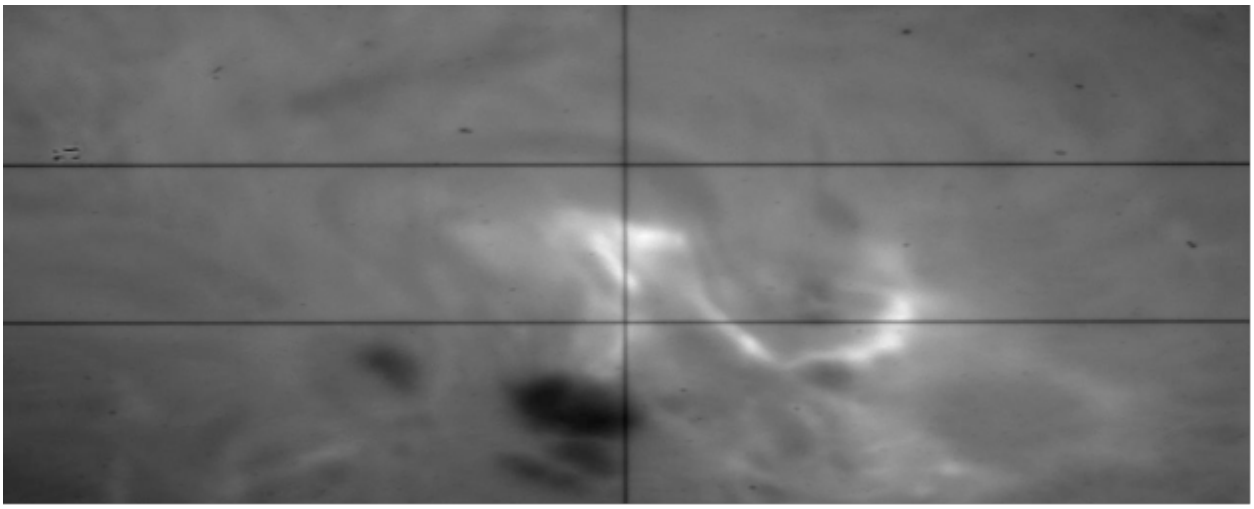

Fig. 1.

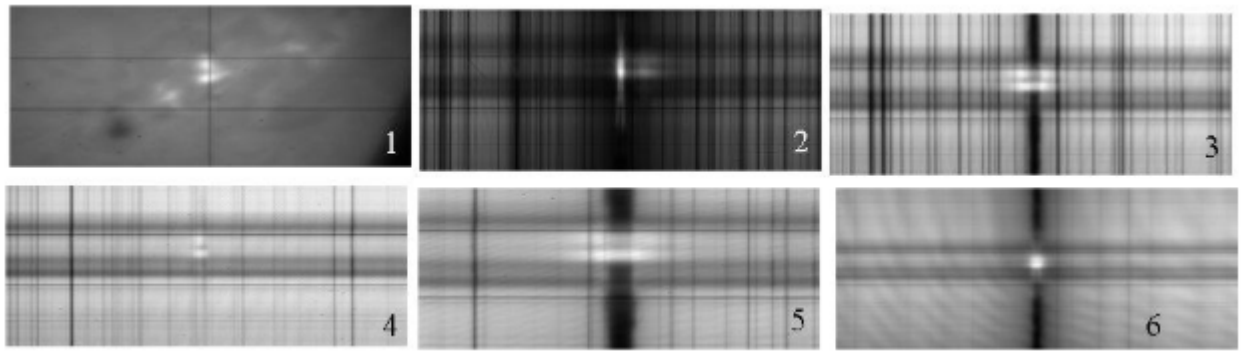
1
2
3
4
5
6

Fig. 2.

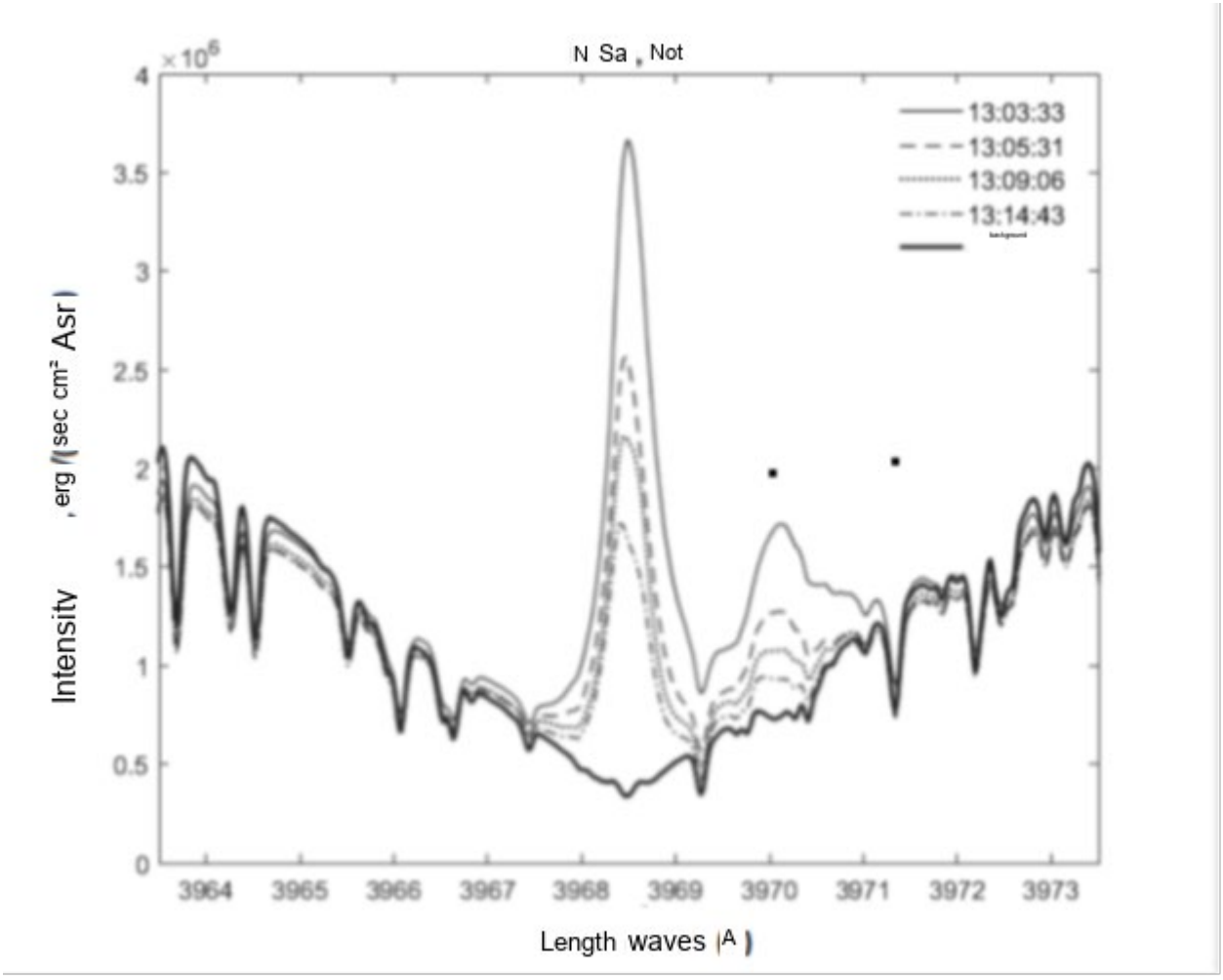
N Sa , Not
×10^6
4
3.5
3
2.5
2
1.5
1
0.5
0
13:03:33
13:05:31
13:09:06
13:14:43
Intensity , erg /(sec cm² Asr)
3964
3965
3966
3967
3968
3969
3970
3971
3972
3973
Length waves (A)

Fig. 3.

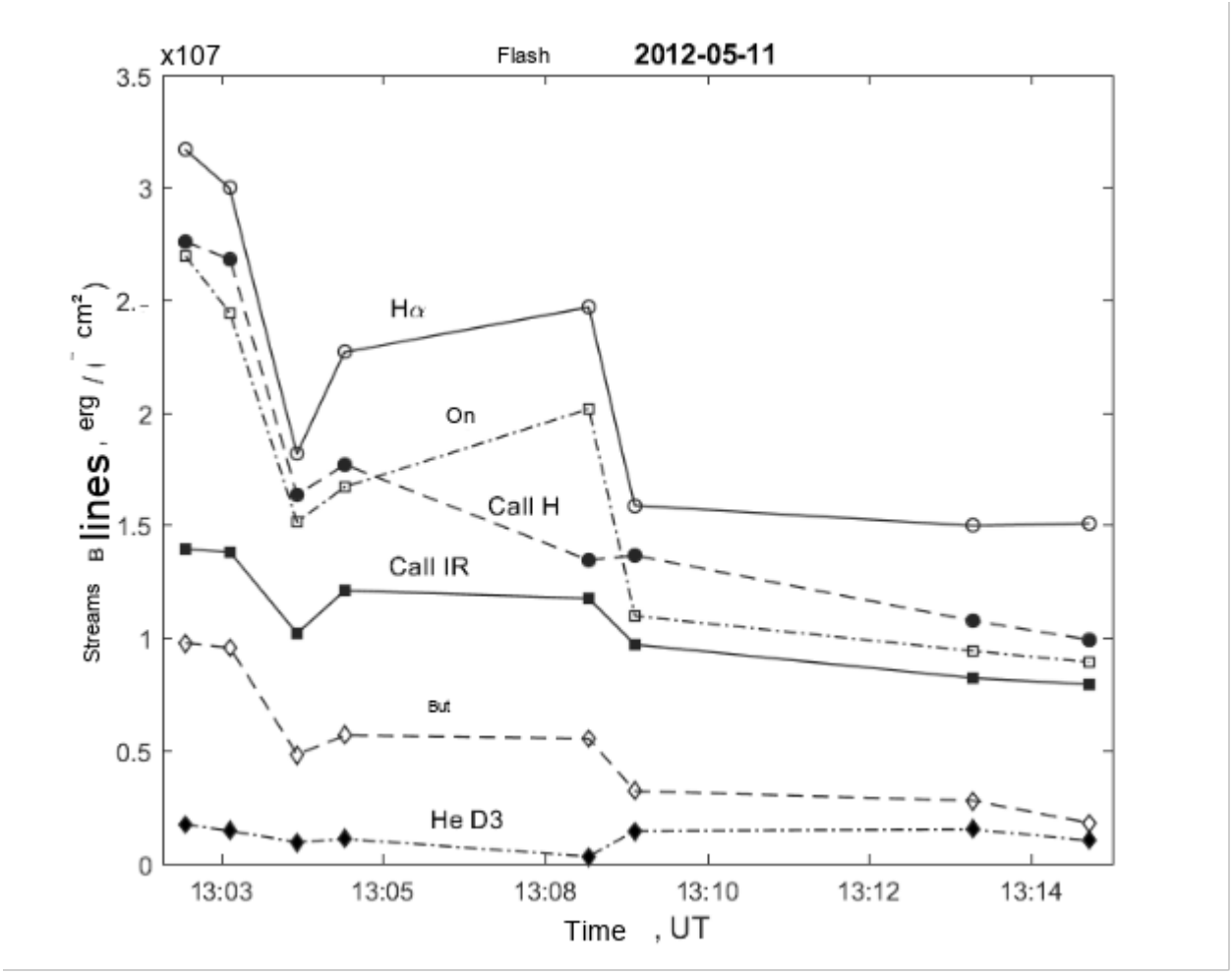
x107
Flash
2012-05-11
3.5
3
2.5
2
1.5
1
0.5
0
Streams B lines, erg / (cm²)
Hα
On
Call H
Call IR
But
He D3
13:03
13:05
13:08
13:10
13:12
13:14
Time , UT

Fig. 4.

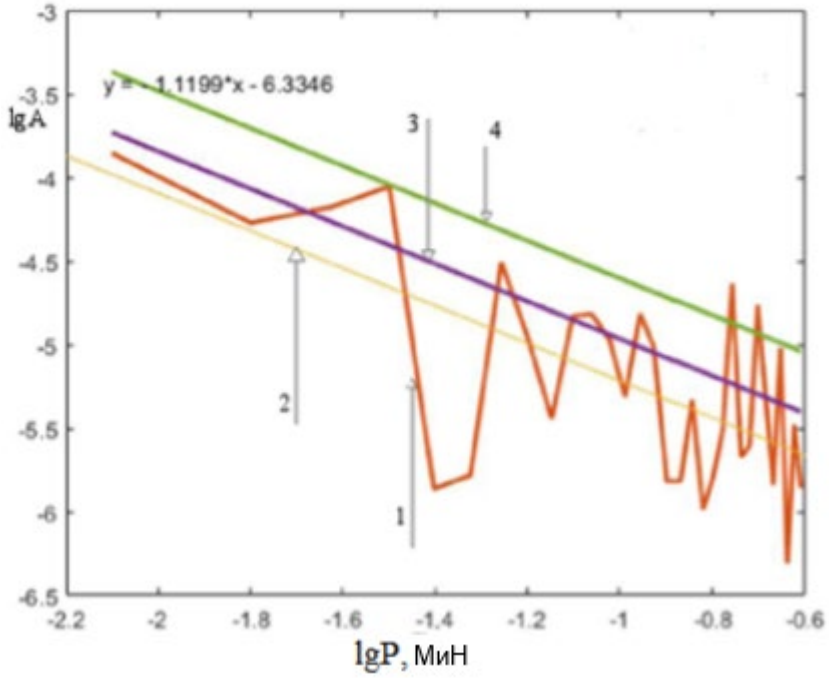
y = -1.1199*x - 6.3346
lgA
lgP, мин
1
2
3
4
-3
-3.5
-4
-4.5
-5
-5.5
-6
-6.5
-2.2
-2
-1.8
-1.6
-1.4
-1.2
-1
-0.8
-0.6

Fig. 5.

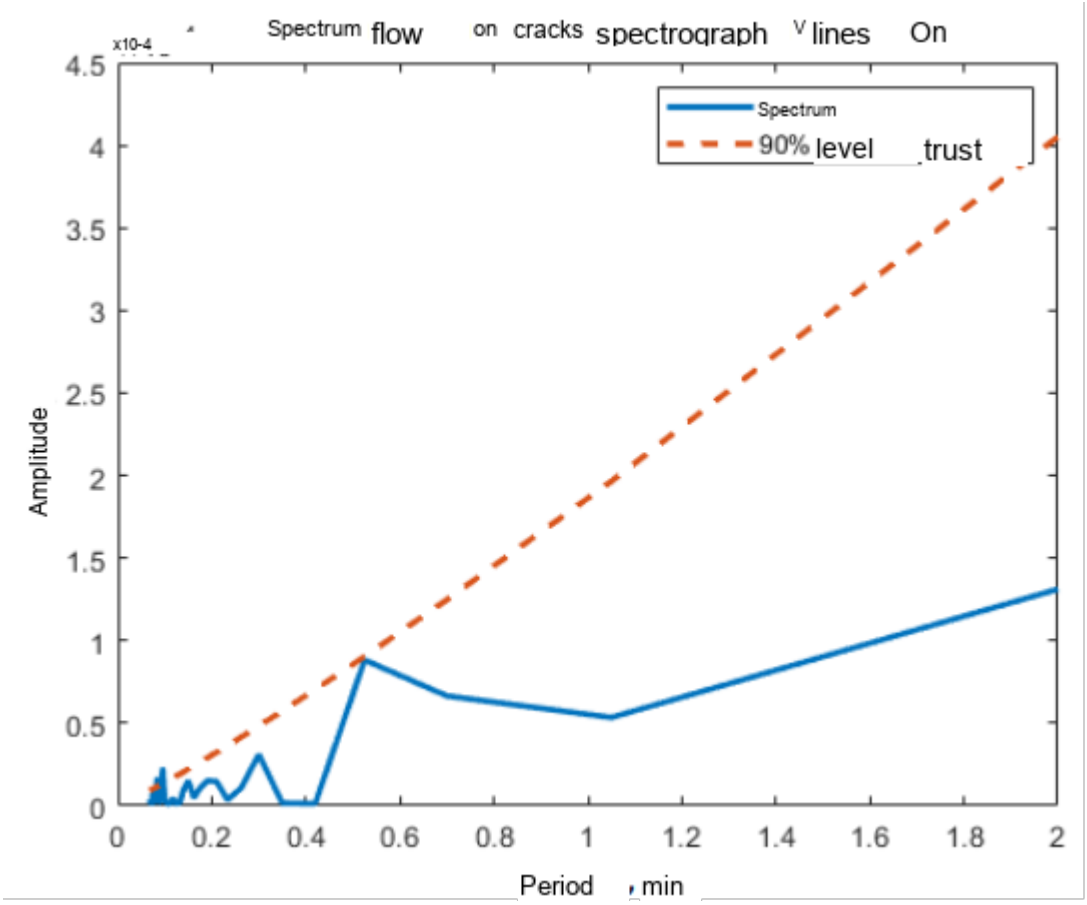
Spectrum flow on cracks spectrograph lines On
x10-4
Spectrum
90% level trust
Amplitude
Period min
0
0.5
1
1.5
2
2.5
3
3.5
4
4.5
0.2
0.4
0.6
0.8
1.2
1.4
1.6
1.8

Fig. 6.